Geoenvironmental Disasters

RESEARCH

Open Access

The study of soft soil seismic subsidence based on the 3D OpenSees model

Ping Li[1,2,4*], Junru Gu[3], Yingci Liu[2,4] and Yuying Li[2,4]

Abstract

Soft soils are characterized by high sensitivity, low strength, and susceptibility to seismic subsidence. In this study, nonlinear dynamic finite element analysis was performed using the OpenSees numerical simulation method to evaluate the seismic subsidence response of soft soil sites to ground motions. Higher peak acceleration of ground motion was found to enhance the degree of uneven seismic subsidence, depth of the seismic depression, and damage to the horizontal surface. The frequency characteristic of ground motion is another factor that influences the seismic subsidence of soft soil. Ground motions with low-frequency contents or high amplitudes lead to a more pronounced seismic subsidence of soft soil, particularly in the case of ground motion that exhibits frequency predominantly close to one of the soil sites. The findings of this study expand the current understanding of seismic subsidence of soft soil.

Keywords: Ground motion, Soft soil, Seismic subsidence, Peak ground acceleration, Frequency

Introduction

Earthquakes often induce massive landslides, collapse, debris flow, liquefaction, and other geological disasters (Subedi and Acharya 2022; Serikawa et al. 2019; Wang et al. 2014). The seismic subsidence of soft soil is a phenomenon where the ground or foundation subsides due to earthquake-induced softening of soft soil. It is one of the most significant earthquake-related hazards that takes place in soft soil areas (Wood 1908; Seed 1990; Mendoza and Romo 1989). For instance, the 1976 Tangshan earthquake in China resulted in the subsidence of buildings on soft clay foundations near Tianjin city, bringing about the maximum settlement and inclination of 380 mm and 3%, respectively (Liu 1986). In 1985, a devastating earthquake hit Mexico City and a large number of buildings that were on soft soil were affected. Some buildings partially sunk to a lower level and others' foundations overturned (IEM 1979). According to Girault (1986), 25 buildings on mat foundations that were supported by friction piles experienced large settlements up to 1.3 m. These historical records indicate that earthquake-related damage, especially in soft soil areas, is primarily generated by seismic subsidence. To mitigate such damage, it is therefore important to investigate the mechanism of soft soil subsidence induced by ground motion.

Factors that influence the seismic subsidence of soft soil have been extensively investigated. Seed and Chan (1966) found that soil samples that were consolidated under static pressure produced additional deformation under dynamic stress. Yu and Shi (1989) claimed that soil seismic subsidence was related to the amplitude of dynamic stress, vibration time, consolidation stress, and soil type. Chen (2004) reported that the seismic settlement of a foundation was related to base pressure, ground motion intensity, foundation size, buried depth of foundation, and foundation type. Meng and Yuan (2004) proposed that subsidence the uneven seismic subsidence of buildings is a result of the combined effect of soft soil layers, uneven load distribution of buildings, and ground motion waveforms. Among these factors, the authors pointed out that the asymmetry and irregularity of ground motion waveforms were the most important factors contributing towards uneven seismic subsidence. Using centrifuge analysis on soft solid foundation, Zhou and Chen

*Correspondence: chinaliping1981@126.com
[1] Hebei Key Laboratory of Earthquake Disaster Prevention and Risk Assessment, Sanhe 065201, China
Full list of author information is available at the end of the article

(2009) indicated that structural asymmetry and building overburden loads promoted uneven seismic subsidence. Li (2002) reported that the subsidence of soft soil was affected by the amplitude of ground motion, site conditions, and overburden loads. Therefore, based on current studies, parameters encompassing upper load, soil layer characteristics, ground motion characteristics, and site characteristics were regarded to be the influencing factors of the seismic subsidence of soft soil. However, some factors continue to lack in-depth investigations and interpretations on ground motion characteristics in particular. Given the complex properties of saturated soft clay, such as high sensitivity, strong compressibility, low water permeability, and low strength, there is extensive evidence on the effects of ground motion characteristics on the seismic subsidence of soft soil. Therefore, the OpenSees finite element analysis software was adopted to build a three-dimensional model of a soft soil site. This was used to study the effect of peak acceleration and frequency characteristics of ground motion on soft soil subsidence. The findings of this study will enhance our existing understanding of the mechanism of soft soil subsidence and serve as a guide for the future seismic design of soft soil foundations.

Methodology

Modelling of a three-dimensional soft soil site

The schematic diagram of a three-dimensional model of the soft soil site is presented in Fig. 1. The dimensions of the site are 30 m (length) × 30 m (width) × 12 m (height) (Liao 1997). The sizes of the horizontal and vertical grid are determined to be 1 m and 0.5 m, respectively. A three-story frame structure exerts a load of 80 kPa on the upper section of the site. The structure constitutes a full, simplified, three-dimensional model of a soft soil site. A rigid boundary is selected for the bottom of the model, and an undrained boundary is set on the surface. The upper and bottom boundaries of the model and foundation-foundation contact surface adopt forced displacement boundaries to keep the soil around the model and in contact with the foundation-foundation boundary to maintain synchronous displacement.

The three-dimensional model adopts the Pressure Independent Multi-Yield (PIMY) soil constitutive model, and the soil particle is simulated by a twenty-node hexahedron that is based on Biot's porous media theory. Empirical parameters of soft soil are calculated and presented in Table 1 (Yang et al. 2004). Initially, the elasticity of the initial ground stress field was calculated by applying gravity. Subsequently, the UpdateMaterial command was applied to calculate permanent deformation. The

Table 1 Empirical parameter values of the soft soil site model

Parameter	Value
Density (kg/m^3)	1300
Shear modulus (kPa)	1.3×10^4
Bulk modulus (kPa)	6.5×10^4
Cohesion (kPa)	18
Peak shear strain	0.1
Friction angle (°)	0
Confining pressure (kPa)	100

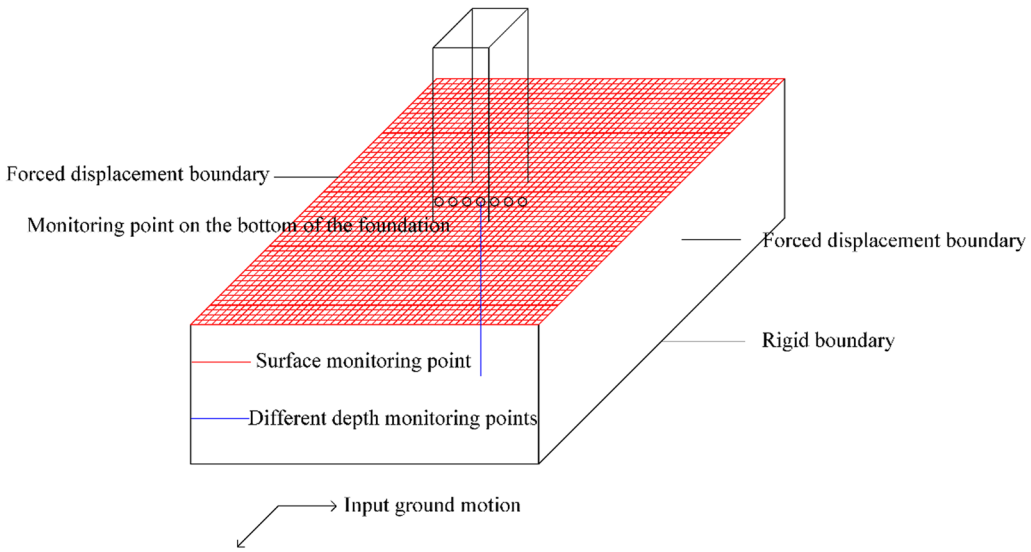

Fig. 1 Schematic diagram of a three-dimensional model of soft soil site

ground motion load was eventually imposed for dynamic analysis.

Input ground motion

A consistent excitation method was selected to apply the El Centro ground motion (Imperial Valley earthquake 1940) at the bottom of the model, considering the vertical propagation of ground motion. The time history curve and Fourier spectrum of the ground motion is demonstrated in Fig. 2. The peak ground acceleration (PGA) of 0.319 g can be observed at 2.02 s and the main frequency is below 10 Hz. The amplitude of the Fourier spectrum is situated between 1–2 Hz. To study the impact of PGA on soft soil subsidence, the PGA of El Centro ground motion were adjusted to 0.15 g, 0.30 g, and 0.40 g.

In addition to El Centro ground motion, two similarly popular ground motions (Kobe and Taft) were incorporated to study the influence of frequency characteristics of ground motion on soft soil subsidence. The PGA of Kobe and Taft ground motions were adjusted to 0.30 g to perform numerical simulations. The time history curve and Fourier spectrum of the Kobe ground motion (Hyogoken-Nanbu earthquake 1995) are shown in Fig. 3. On the other hand, the time history curve and Fourier spectrum of the Taft ground motion (California earthquake 1952) are presented in Fig. 4. Fourier spectra of Kobe and

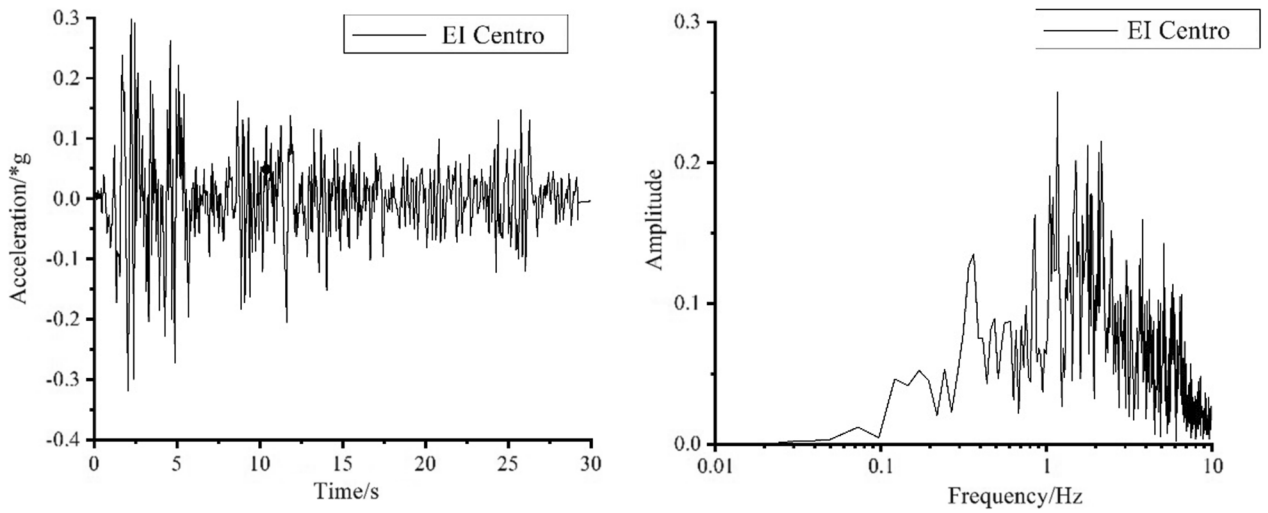

Fig. 2 Time history curve and Fourier spectrum of El Centro ground motion

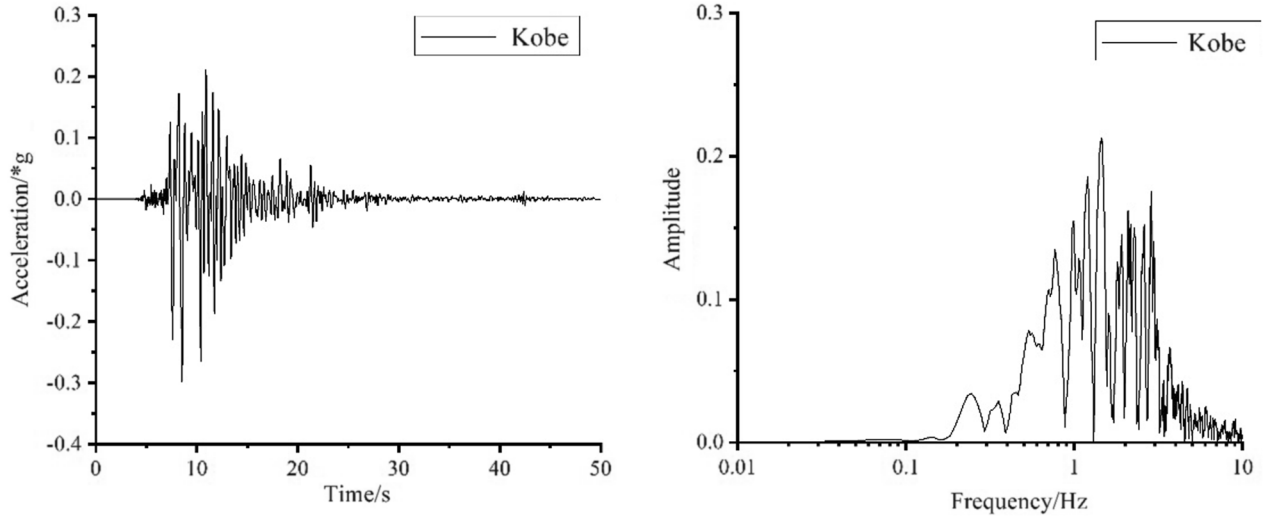

Fig. 3 Time history curve and Fourier spectrum of Kobe ground motion

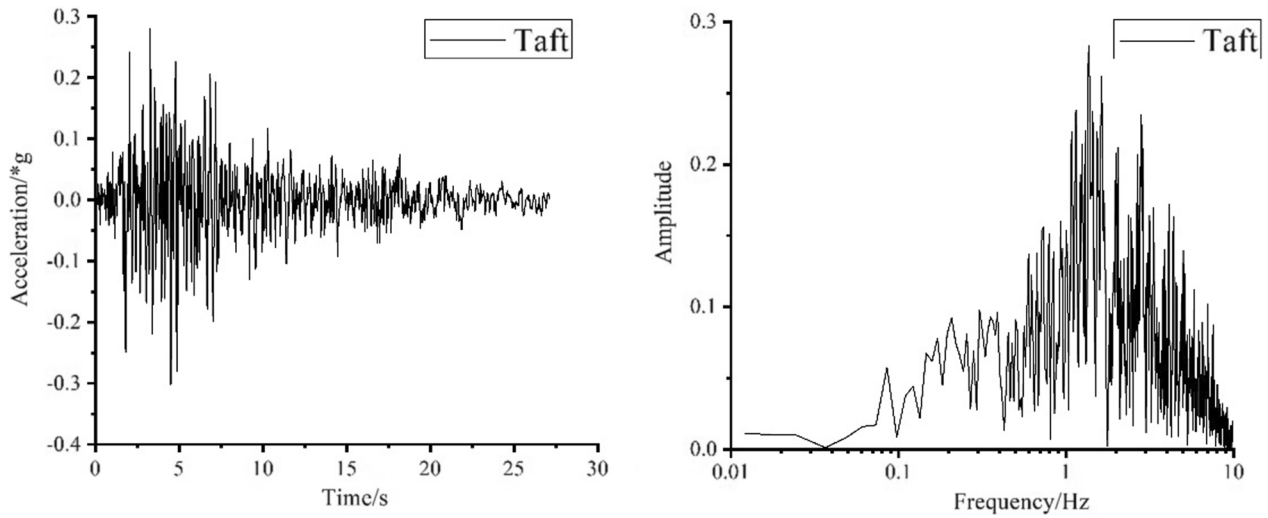

Fig. 4 Time history curve and Fourier spectrum of Taft ground motion

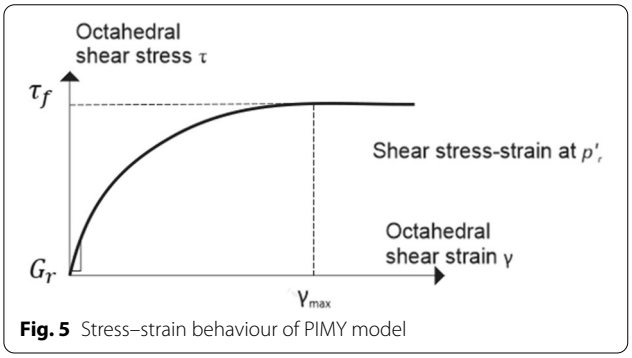

Fig. 5 Stress–strain behaviour of PIMY model

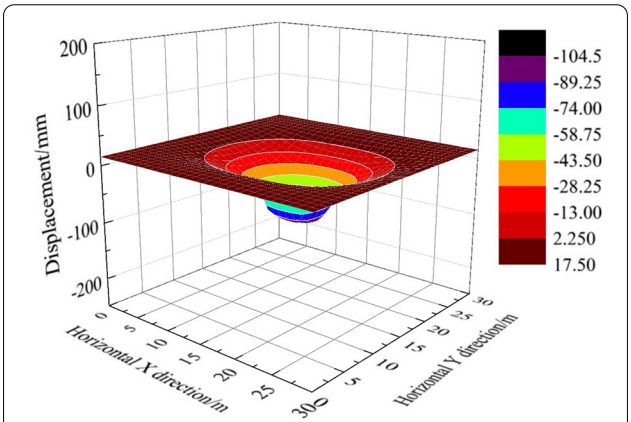

Fig. 6 Seismic subsidence of ground surface due to 0.15 g El Centro ground motion (full view)

Taft ground motion are dominated by low frequencies of below 5 Hz and 8 Hz, respectively.

Methods of analysis

OpenSees is an object-oriented, open-source finite element analysis software widely used in earthquake engineering. OpenSees is open source, and users can select or re-develop available constitutive models, unit forms, and solution algorithms.

In this study, the PIMY model was selected as the soil constitutive model to illustrate the plasticity of elasto-plastic materials under deviatoric stress–strain conditions. The model exhibits linear-elastic volumetric stress–strain response and is not affected by the deviatoric response. The response of the materials, of which shear behaviour is not sensitive to confinement changes and monotonic or cyclic loading, can be simulated by the PIMY model (Yang et al. 2003).

Figure 5 shows the stress–strain behaviour of the PIMY model. When applying the gravity load (i.e., the consolidation stage), the model exhibits linear elasticity. During the subsequent dynamic loading stage, the model demonstrates an elastoplastic stress–strain response. The plasticity of the model is calculated using the multiple yield surface principle and corresponding flow law. The yield surface obeys the Von Mises yield criterion.

Results and discussion

Influence of PGA of ground motion on the seismic subsidence of soft soil

The vertical displacement of soil due to the El Centro ground motion with a PGA of 0.15 g was calculated at the bottom of the foundation for each monitoring point. Figures 6 and 7 show the seismic subsidence of the ground surface derived from the dynamic calculation of the

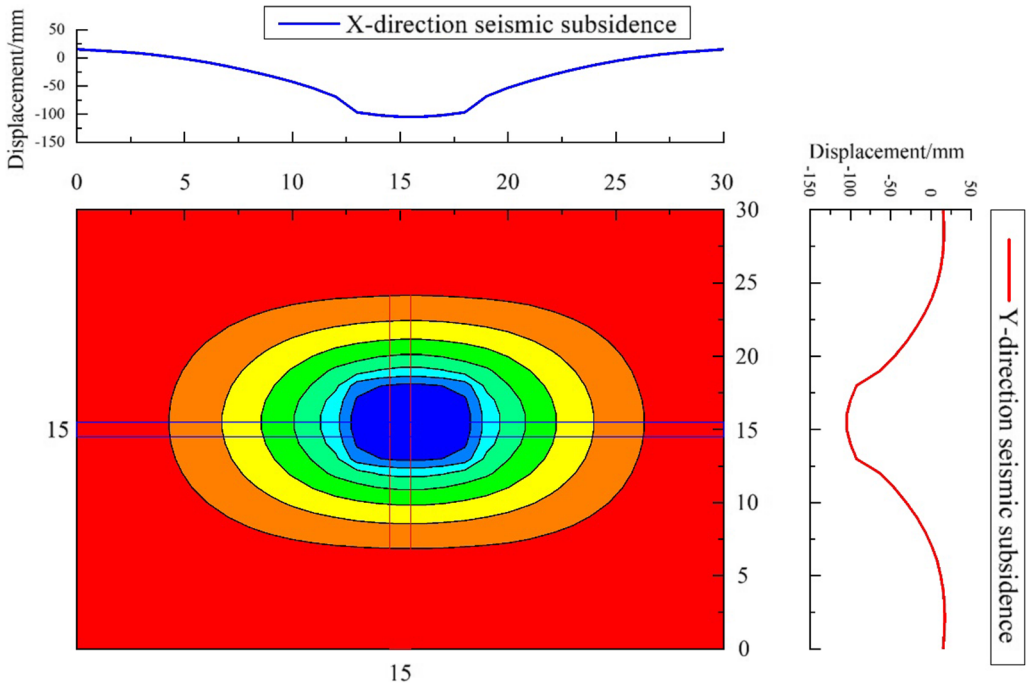

Fig. 7 Seismic subsidence of ground surface due to 0.15 g El Centro ground motion (cross-sectional view)

three-dimensional model of the soft soil site. Figure 6 indicates that the seismic subsidence propagates from the centre, where the most significant seismic displacement is observed, and gradually decreases until reaching the ground surface where significant plastic deformation and shear failure were observed. Figure 7 illustrates the cross-sectional view of the foundation after seismic subsidence. Propagation of the seismic subsidence assumes a parabolic shape that is symmetrically distributed on the low, middle, and high sides with a maximum depression angle of 3.44°. The largest vertical displacement is observed at the bottom centre of the foundation. The impact boundary of the seismic subsidence is shown as an ellipse spanning from 5 to 25 m in X-direction and 6–24 m in Y-direction. The soil in both the X-direction and Y-direction of the foundation is compressed and uplifted by 15 mm.

The vertical displacement of soil due to the El Centro ground motion with a PGA of 0.30 g was calculated at the bottom of the foundation for each monitoring point. Figures 8 and 9 show the seismic subsidence of the ground surface obtained from the dynamic analysis of the three-dimensional model of the soft soil site. Figure 8 indicates that seismic subsidence spreads from the centre, where the largest subsidence is observed,

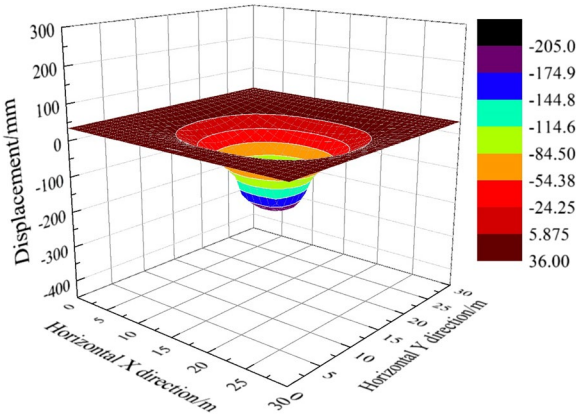

Fig. 8 Seismic subsidence of ground surface due to 0.30 g El Centro ground motion (full view)

and gradually decreases until reaching the ground surface where significant plastic deformation and shear failure were recorded. Figure 9 illustrates the cross-sectional view of the foundation after seismic subsidence. Propagation of the seismic subsidence follows a parabolic shape that is symmetrically distributed on the low, middle, and high sides with a maximum depression

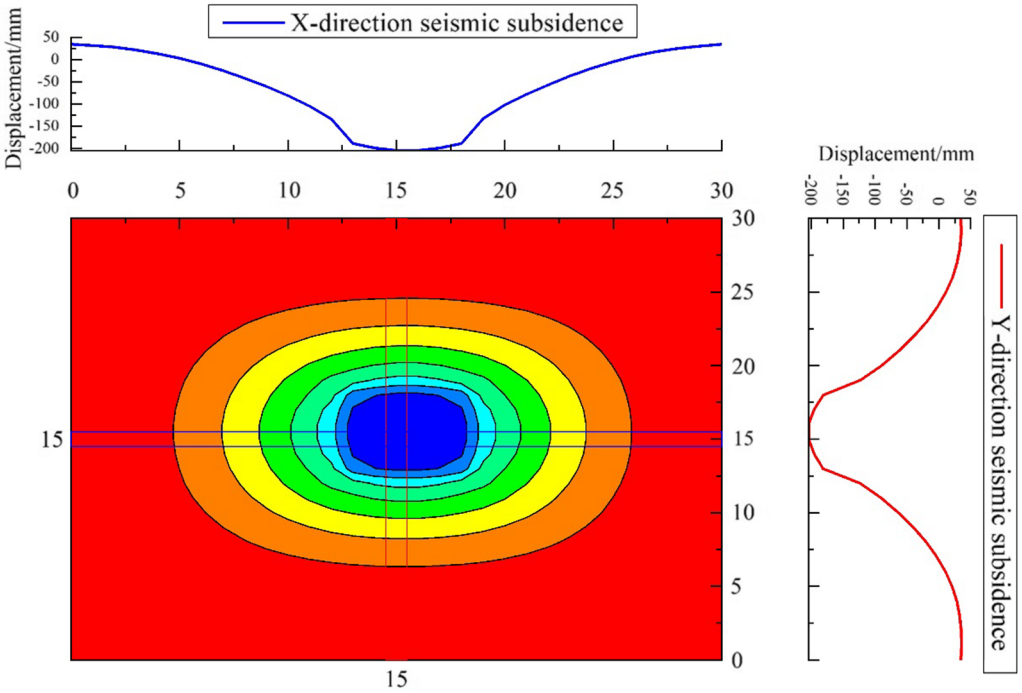

Fig. 9 Seismic subsidence of ground surface due to 0.30 g El Centro ground motion (cross-sectional view)

angle of 7.91°. The middle bottom of the foundation demonstrates the largest amount of vertical displacement. The impact boundary of the seismic subsidence is shown as an ellipse, covering from 4.5 to 25.5 m in X-direction and 6.5–24.5 m in Y-direction. The soil in both the X-direction and Y-direction of the foundation is compressed and uplifted by 35 mm.

The vertical displacement of soil due to the El Centro ground motion with a PGA of 0.40 g was calculated at the bottom of the foundation for each monitoring point. Figures 10 and 11 show the seismic subsidence of the ground surface derived from the dynamic calculation on the three-dimensional model of the soft soil site. Figure 10 implies that the seismic subsidence propagates from the centre, where the most significant seismic subsidence is recorded, and gradually decreases until the ground surface where significant plastic deformation and shear failure are detected. Figure 11 illustrates the cross-sectional view of the foundation after seismic subsidence. Propagation of the seismic subsidence assumes a parabolic shape symmetrically distributed on the low, middle, and high sides with a maximum depression angle of 8.0°. The bottom centre of the foundation exhibits the largest vertical displacement. The impact boundary of the seismic subsidence is shown as an ellipse ranging from 4.5 to 26.0 m in X-direction and 6.0–25.0 m in Y-direction. The soil in both the X-direction and Y-direction of the foundation are compressed and uplifted by 46 mm.

The overall effects of PGA on seismic subsidence of soft soil are summarized in Figs. 12, 13 and 14. As shown in Fig. 12, seismic subsidence that is generated by 0.15 g ground motion is approximately 104 mm, which is 80.6% and 148.6% lower than the subsidence generated under 0.30 g and 0.40 g ground motion (189 mm and 260 mm). This indicates that an increase in PGA distinctly expands the degree of seismic subsidence. Figure 13 illustrates the development of seismic subsidence at different depths of soil. A lower seismic subsidence is observed at the deeper soil layer. Nevertheless, 0.40 g ground motion produces a notably higher seismic subsidence than 0.15 g and 0.30 g of ground motion regardless of the soil depth, which indicates a non-linear stress–strain response of the soil.

The PGA of ground motion influences uneven surface subsidence. As shown in Fig. 14, a larger PGA leads to a

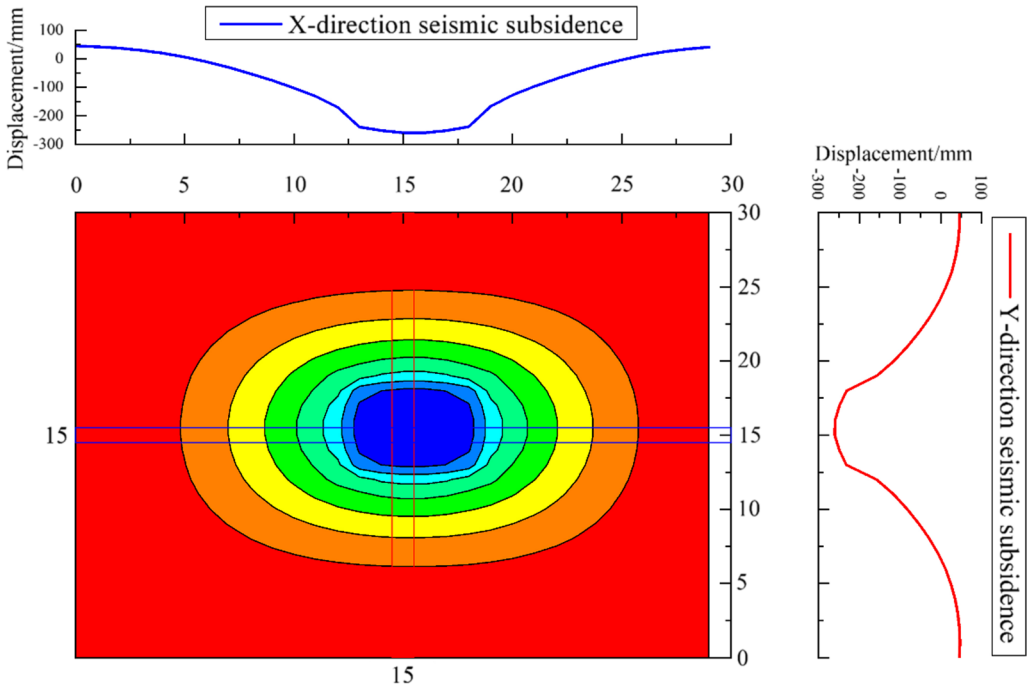

Fig. 10 Seismic subsidence of ground surface due to 0.40 g El Centro ground motion (full view)

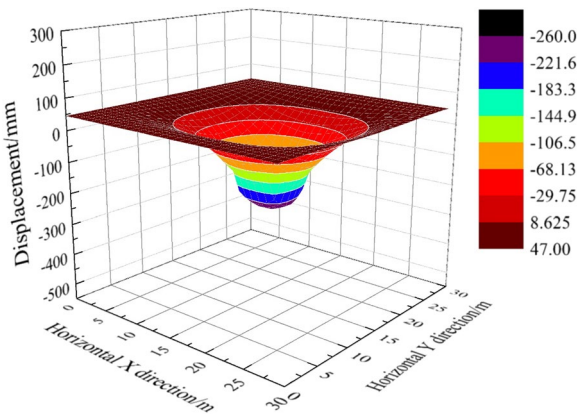

Fig. 11 Seismic subsidence of ground surface due to 0.40 g El Centro ground motion (cross-sectional view)

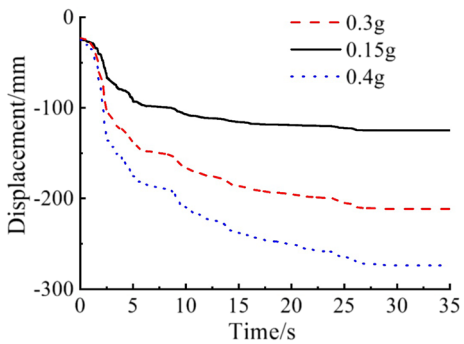

Fig. 12 Time history curve illustrating vertical subsidence of soil due to El Centro ground motion with various PGA

more significant subsidence, a higher uplifted distance of soil in both the X-direction and Y-direction of the foundation, as well as a larger distance of damage on a horizontal surface. The impact of seismic subsidence in X-direction is larger than that of the Y-direction, which is observed as a consequence of the X-direction to which ground motion is applied.

Influence of frequency characteristics of ground motion on seismic subsidence of soft soil

Figures 15 and 16 show the seismic subsidence of the ground surface, which is derived from the dynamic calculation on the three-dimensional model of the soft soil site. The seismic subsidence propagates from the centre, where the largest subsidence is observed, and gradually decreases until reaching the ground surface at which significant plastic deformation and shear failure were indicated (Fig. 15). Figure 16 illustrates the cross-section of the foundation after seismic subsidence. Propagation of

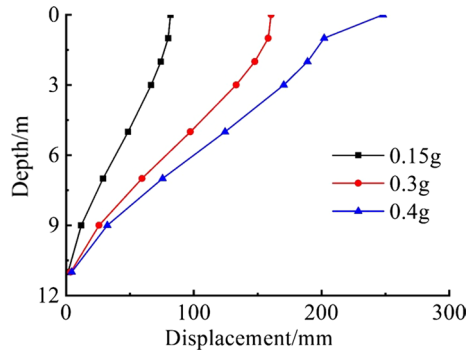

Fig. 13 Seismic subsidence at different soil depths due to El Centro ground motion with different PGA

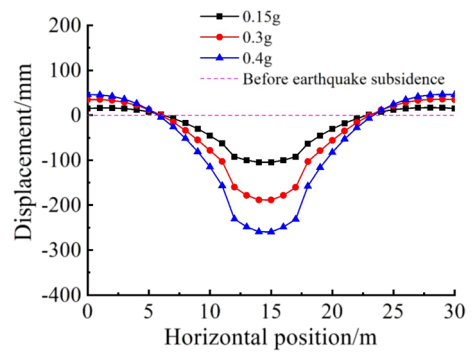

Fig. 14 Uneven seismic subsidence of ground surface due to El Centro ground motion with different PGA

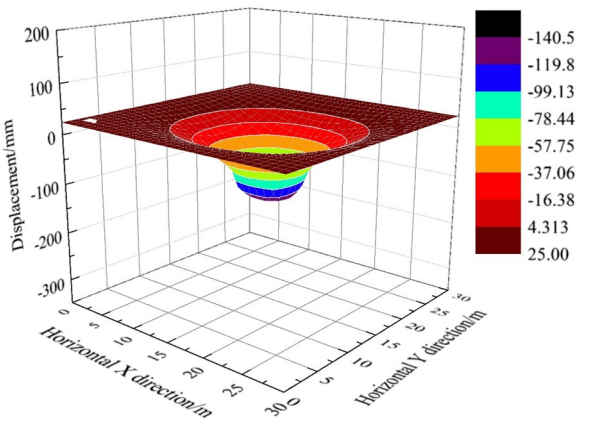

Fig. 15 Seismic subsidence of ground surface due to 0.30 g Kobe ground motion (full view)

the subsidence adopts a parabolic shape that is symmetrically distributed on the low, middle, and high sides with a maximum depression angle of 5.01°. The largest displacement was found at the bottom middle of the foundation. The impact boundary of subsidence is shown as an ellipse spanning from 4.5 to 25.5 m in X-direction and 6.0–25.0 m in the Y-direction. The soil in both the directions of the foundation is compressed and uplifted by 24 mm.

The vertical displacement of soil due to the Taft ground motion with a PGA of 0.30 g was calculated at the bottom of the foundation for each monitoring point. Figures 17 and 18 show the seismic subsidence of ground surface derived from the dynamic calculation on a three-dimensional model of the soft soil site. Figure 17 indicates that the seismic subsidence spreads from the centre, where the largest subsidence is observed, and gradually decreases until the ground surface at which plastic deformation and shear failure is recorded. Figure 18 illustrates the cross-sectional view of the foundation after seismic subsidence. The subsidence adopts a parabolic shape that is symmetrically distributed on the low, middle, and high sides with a maximum depression angle of 7.66°. The largest vertical displacement was observed at the bottom middle of the foundation. The impact boundary of the seismic subsidence is shown as an ellipse ranging from 4.5 to 26.0 m in X-direction and 6.5–25.0 m in Y-direction. The soil in both the X-direction and Y-direction of the foundation is compressed and uplifted by 44 mm.

The overall effects of frequency characteristics of ground motion on seismic subsidence of soft soil are summarized in Figs. 19, 20 and 21. Figure 19 shows the different growth characteristics of vertical displacement that is produced by three ground motions (El Centro, Kobe, and Taft). Soil subsidence is initiated at 7 s by Kobe ground motion, which was consistent with the onset time at which the PGA of Kobe ground motion was recorded. Figure 20 shows the development of seismic subsidence at different depths of soil. Regardless of this, Taft ground motion demonstrates the most significant seismic subsidence and is followed by El Centro and Kobe ground mot ion.

Figure 21 indicates that the three ground motions generated different degrees of seismic subsidence, which further suggests the degree of influence of frequency characteristics of ground motions on the seismic subsidence of soft soil. The natural frequency of the model site is 1.2 Hz. Similarly, the amplitude of the Fourier spectrum of the Taft ground motion is located at 1–2 Hz, which is close to the natural frequency of the site. This resonance significantly increases the vertical displacement of the soil. Despite exhibiting many low-frequency properties similar to the Taft ground motion, El Centro and Kobe ground motions demonstrate lower amplitudes than Taft ground motion. Therefore, Taft ground motion produced the most severe seismic subsidence of soft soil among the investigated ground motions. Overall, these findings highlight the significance of low-frequency

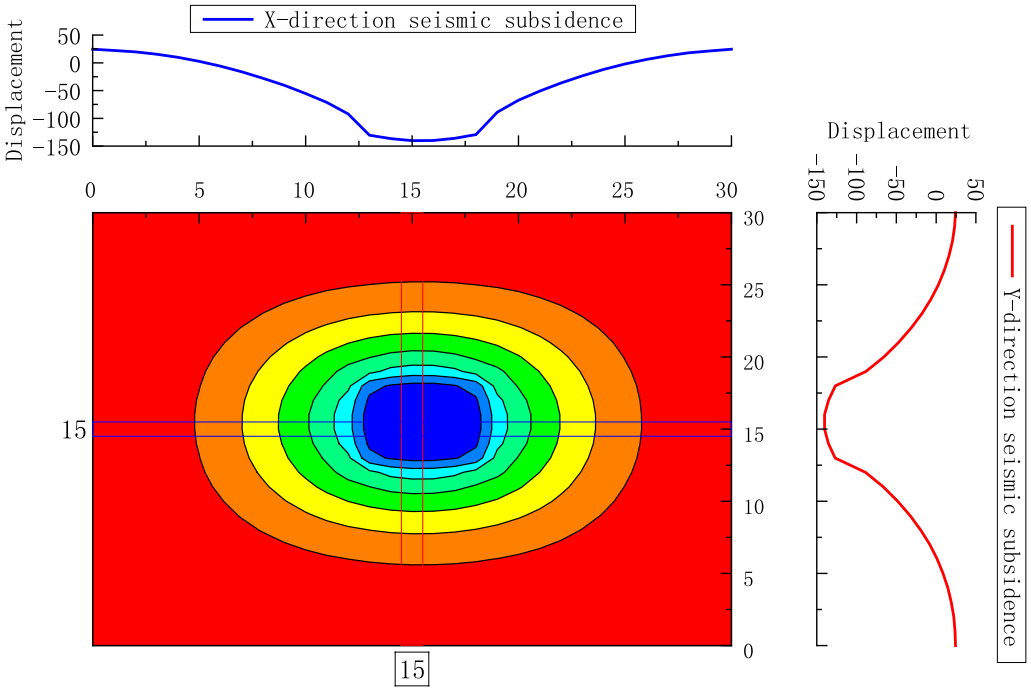

Fig. 16 Seismic subsidence of ground surface due to 0.30 g Kobe ground motion (cross-sectional view)

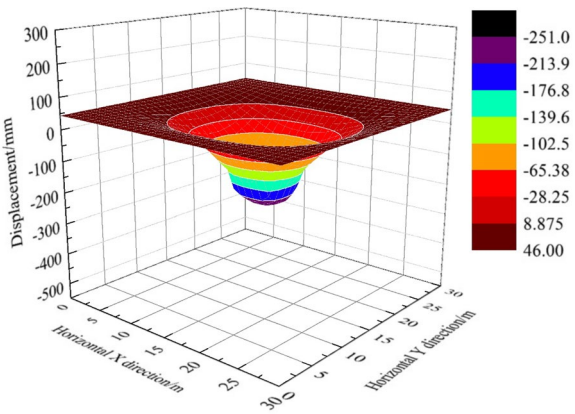

Fig. 17 Seismic subsidence of ground surface due to 0.30 g Taft ground motion (full view)

contents and the amplitude of the Fourier spectrum on seismic subsidence of soft soil. The higher abundance of low-frequency contents and the higher amplitude of the Fourier spectrum promote increasingly severe seismic subsidence.

Although this study contributes towards understanding the impact of PGA and the frequency characteristics of ground motion on soft soil subsidence, these findings were derived from a simplified three-dimensional model. Hence, some mechanisms and factors related to actual soft soil subsidence during strong earthquakes may not be accounted for by the current model. On this account, a large-scale three-dimensional model that can simulate actual interactions between the foundation and soft soil is necessary to obtain more reliable conclusions from numerical analysis. Moreover, further research that takes into account soft soil properties, upper load, and foundation-soil interaction is encouraged to validate the impact of ground motion characteristics on soft soil and derive the influencing factors of the seismic subsidence of soft soil.

Conclusion

A three-dimensional model of the soft soil site was established, and finite element numerical simulations were carried out to evaluate the influence of PGA and frequency characteristics of ground motion on the seismic subsidence of soft soil. The higher PGA of ground motion increases the degree of seismic subsidence, depth of the seismic depression, and damage to a horizontal surface. The frequency characteristics of ground motion are comparatively important influencing factors of soft soil subsidence. The larger number of low-frequency contents and the higher amplitude of ground motion generate more severe seismic subsidence. Moreover, the more similar the predominant frequency of the ground motion to the natural frequency of the soft soil site, the more significant the seismic subsidence appears to be.

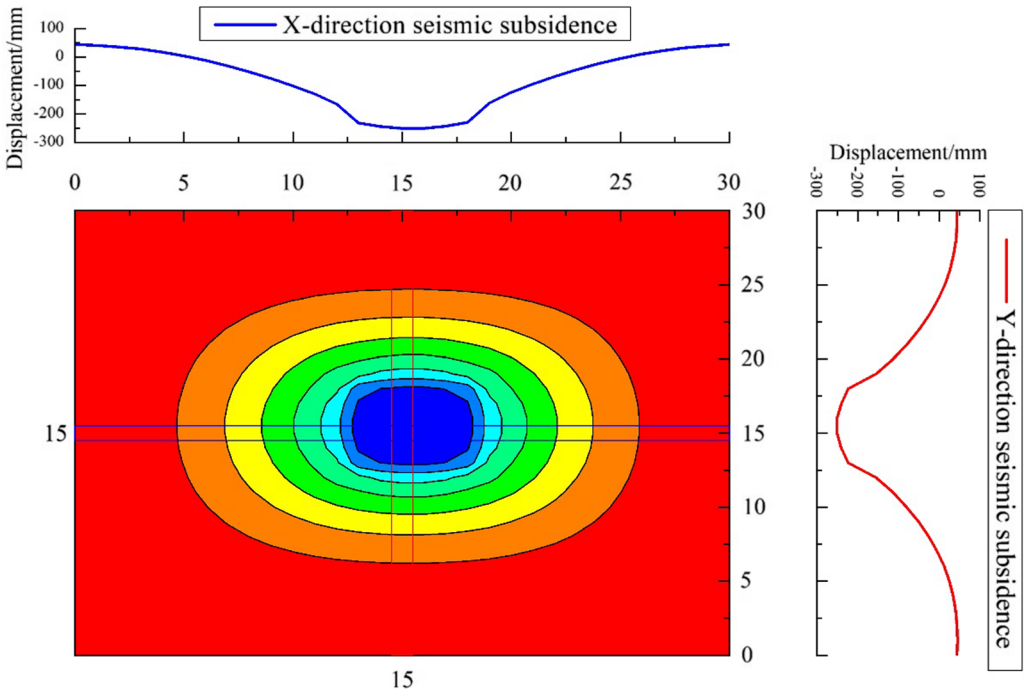

Fig. 18 Seismic subsidence of ground surface due to 0.30 g Taft ground motion (cross-sectional view)

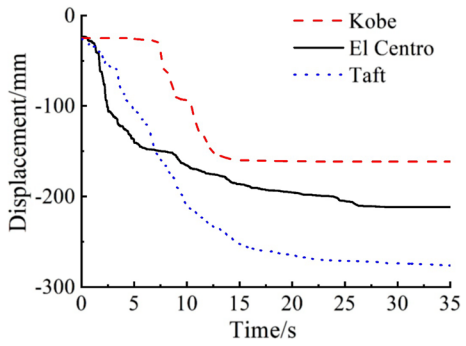

Fig. 19 Time history curve illustrating the vertical subsidence of soil due to different ground motions

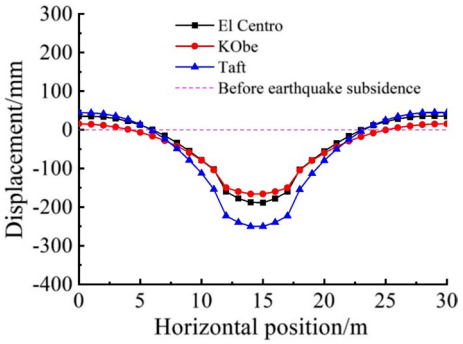

Fig. 21 Seismic subsidence due to different ground motions

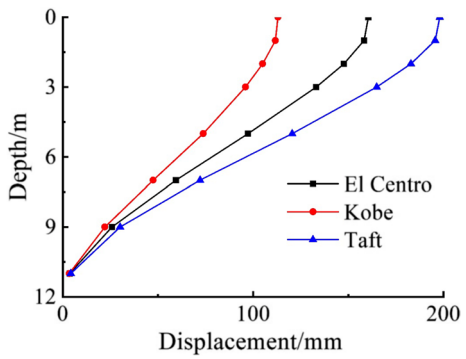

Fig. 20 Seismic subsidence at different soil depths due to different ground motions

Acknowledgements
The authors would like to thank the China Earthquake Administration Spark Project of Earthquake Science and Technology for funding. They would also like to acknowledge OpenSees for providing numerical tools.

Author contributions
PL was involved in simulations and writing the manuscript. All other authors contributed to data analysis, simulations, and paper writing. All the authors read and approved the final manuscript.

Funding
China Earthquake Administration Spark Project of Earthquake Science and Technology (XH204401) has funded the analysis and construction.

Declarations

Competing interests
The authors declare that they have no competing interests.

Author details
[1]Hebei Key Laboratory of Earthquake Disaster Prevention and Risk Assessment, Sanhe 065201, China. [2]Institute of Disaster Prevention, Sanhe 065201, China. [3]Sichuan Metallurgical Geological Survey and Design Group Co., Ltd, Chengdu 610081, China. [4]Key Laboratory of Earthquake Engineering and Engineering Vibration, Institute of Engineering Mechanics, China Earthquake Administration, Harbin 150081, Heilongjiang Province, China.

Received: 10 June 2021 Accepted: 23 April 2022
Published online: 05 May 2022

References

Chen GX (2004) A simplified method for calculating earthquake-induced foundation subsidence of multi-storied buildings and analysis of influencing factors. Journal of Disaster Prevention and Mitigation Engineering 24(1):47–52 (**in Chinese**)
Girault P (1986) Analysis of foundation failures in the Mexico Earthquake, 1985—factors involved and lessons learned. ASCE, pp 178–192
IEM (1979) (Institute of Engineering Mechanics Chinese Academy of Science) Haicheng Earthquake damage. Seismological Press, Beijing, p 635 **(in Chinese)**
Li N (2002) Based on the subsidence of soft soil and its influencing factors of OpenSees research. Institute of Engineering Mechanics China Earthquake Administration, Haerbin (**in Chinese**)
Liao ZP (1997) Numerical simulation of near-field wave. Adv Mech 27(2):193–212 (**in Chinese**)
Liu HX (1986) Tangshan Earthquake damage. Seismological Press, Beijing, p 436 (**in Chinese**)
Mendoza M, Romo M (1989) Behavior of building foundations in Mexico City during the 1985 Earthquake: second stage. In: Proc., Lessons Learned from the 1985 Mexico Earthquake, pp 66–70
Meng SJ, Yuan XM (2004) The research to the influential factors of differential subsidence of buildings. Earthq Eng Eng Vib 24(1):111–116 (**in Chinese**)
Seed HB, Chan CK (1966) Clay strength under earthquake loading condition. J Soil Mech Found Div 92(2):53–78
Seed RB (1990) Preliminary report on the principal geotechnical aspects of the October 17, 1989, Loma Prieta Earthquake Report No. UCB/EERC-90/05
Serikawa Y, Miyajima M, Yoshida M, Matsuno K (2019) Inclination of houses induced by liquefaction in the 2018 Hokkaido Iburi-tobu earthquake, Japan. Geoenviron Disasters 6(14):1–9
Subedi M, Acharya P (2022) Liquefaction hazard assessment and ground failure probability analysis in the Kathmandu Valley of Nepal. Geoenviron Disasters 9(1):1–17
Wang FW, Sun P, Highland L, Cheng QG (2014) Key factors influencing the mechanism of rapid and long runout landslides triggered by the 2008 Wenchuan earthquake, China. Geoenviron Disasters 1(1):1–16
Wood HO (1908) Distribution of apparent intensity in San Francisco. The California Earthquake of April, 18(1906), pp 220–227
Yang Z, Elgamal A, Parra E (2003) Computational model for cyclic mobility and associated shear deformation. J Geotech Geoenviron Eng 129(12):1119–1127
Yang Z, Lu J, Elgamal A (2004) A web-based platform for live internet computation of seismic ground response. Adv Eng Softw 35:249–259
Yu SS, Shi ZJ (1989) The soil subsidence of experimental research. Chin J Geotech Eng 11(4):35–44 (**in Chinese**)
Zhou YG, Chen YM (2009) Building on soft clay foundation uneven settlement centrifuge test research. Chin Sci 39(6):1129–1137 (**in Chinese**)

Publisher's Note